Channels

ISSN: 1933-6950 (Print) 1933-6969 (Online) Journal homepage: https://www.tandfonline.com/loi/kchl20

Dynamical characterization of inactivation path in voltage-gated Na^+ ion channel by non-equilibrium response spectroscopy

Krishnendu Pal & Gautam Gangopadhyay

To cite this article: Krishnendu Pal & Gautam Gangopadhyay (2016) Dynamical characterization of inactivation path in voltage-gated Na^+ ion channel by non-equilibrium response spectroscopy, Channels, 10:6, 478-497, DOI: 10.1080/19336950.2016.1205175

To link to this article: https://doi.org/10.1080/19336950.2016.1205175

Published online: 26 Jul 2016.

CHANNELS
2016, VOL. 10, NO. 6, 478–497
http://dx.doi.org/10.1080/19336950.2016.1205175

Taylor & Francis
Taylor & Francis Group

RESEARCH PAPER

Dynamical characterization of inactivation path in voltage-gated Na^+ ion channel by non-equilibrium response spectroscopy

Krishnendu Pal and Gautam Gangopadhyay

Chemical Biological and Macromolecular Sciences, S.N. Bose National Center for Basic Sciences, Kolkata, India

ABSTRACT

Inactivation path of voltage gated sodium channel has been studied here under various voltage protocols as it is the main governing factor for the periodic occurrence and shape of the action potential. These voltage protocols actually serve as non-equilibrium response spectroscopic tools to study the ion channel in non-equilibrium environment. In contrast to a lot of effort in finding the crystal structure based molecular mechanism of closed-state(CSI) and open-state inactivation(OSI); here our approach is to understand the dynamical characterization of inactivation. The kinetic flux as well as energetic contribution of the closed and open- state inactivation path is compared here for voltage protocols, namely constant, pulsed and oscillating. The non-equilibrium thermodynamic quantities used in response to these voltage protocols serve as improved characterization tools for theoretical understanding which not only agrees with the previously known kinetic measurements but also predict the energetically optimum processes to sustain the auto-regulatory mechanism of action potential and the consequent inactivation steps needed. The time dependent voltage pattern governs the population of the conformational states which when couple with characteristic rate parameters, the CSI and OSI selectivity arise dynamically to control the inactivation path. Using constant, pulsed and continuous oscillating voltage protocols we have shown that during depolarization the OSI path is more favored path of inactivation however, in the hyper-polarized situation the CSI is favored. It is also shown that the re-factorisation of inactivated sodium channel to resting state occurs via CSI path. Here we have shown how the subtle energetic and entropic cost due to the change in the depolarization magnitude determines the optimum path of inactivation. It is shown that an efficient CSI and OSI dynamical profile in principle can characterize the open-state drug blocking phenomena.

ARTICLE HISTORY
Received 24 February 2016
Revised 27 May 2016
Accepted 19 June 2016

KEYWORDS
characterization of inactivation; closed-state inactivation; inactivation path; non-equilibrium response spectroscopy; open-state inactivation; total entropy contribution

Introduction

Inactivation of sodium ion channel[1,2] is a self-controlled process necessary to sustain the firing pattern of axon potential in excitable tissues.[3-6] In excitable cells like neurons, muscles, cardiac and endocrine cells, the action potential is initiated when a stimulus causes the membrane potential to reach a threshold which subsequently results in depolarization. After the membrane potential reaches a threshold, voltage gated sodium channels open, allowing an influx of positively charged sodium ions into the cell and further depolarize it.[7] When the cell is depolarised enough the inactivation of sodium channel occurs which inhibits the cell from further excitation.[3] Inactivated state of sodium channel temporarily prevents the channel from reopening until the cell is brought back to the resting potential by potassium channel by out-fluxing the K^+ ions from the cell. If this inactivation process is hampered, various physiological problems appear, like cardiac arrest, hyper excitability, hysteria, epilepsy etc.[8-10] The persistent current has special functions associated with this inactivation process, such as integration of synaptic potentials and acceleration of firing rates etc.[11-13] Various mutations and hereditary diseases also affect the proper inactivation process which makes the sodium channel an optimal drug target.[14]

Inactivation of the Na^+ conductance in a squid giant axon was first characterized by Hodgkin and Huxley.[15] Since then a lot of investigation on inactivation of sodium ion channel at the functional and structural levels[4,16-20] had been performed. These studies showed that the inactivation process involves mainly 2

CONTACT Gautam Gangopadhyay gautam@bose.res.in S.N. Bose National Centre For Basic Sciences, Block-JD, Sector-III, Salt Lake, Kolkata-700106, India.
Color versions of one or more of the figures in the article can be found online at www.tandfonline.com/kchl.

distinct and complex molecular mechanisms. The well-known first type of the inactivation is the mechanism that occurs from the open-state, so called open-state inactivation (OSI), at strongly depolarized membrane potentials. The other type of inactivation occurs from pre-open closed states, the closed-state inactivation (CSI), at hyper-polarized and modestly depolarized membrane potentials. Thus voltage-gated Na^+ channel utilizes both OSI and CSI[16,17,21,22] paths. Although detailed mechanistic description of OSI is there,[23] much less is known about the CSI in this regard.[24-26]

For the previous few decades the majority of the studies of inactivation had been performed by elctrophysiologists using usual voltage clamp and patch clamp techniques. But recently developed non-equilibrium response spectroscopic technique[27,28] has become popular method to study the ion channels in non-equilibrium environment,[29] using continuously oscillating voltage protocol[30] or fluctuating voltage[31] or pulse train voltage protocol. This sort of non-equilibrium response spectroscopic technique provides new aspects of ion channel gating kinetics which standard stepped-potential protocols cannot provide.[30] Beside all these although a great deal of effort has been exercised to kinetically understand the molecular mechanism of inactivation, the nonequilibrium thermodynamics in the problems of inactivation has never been applied. The study of nonequilibrium parameters like total entropy production rates can be used to confirm the kinetic results[32] For oscillating voltage protocol, with its biophysically chosen amplitude, frequency and mean voltage, the system replicates the neuronal oscillation which arises due to oscillatory nature of the membrane depolarization. Also the pulse train protocol is applied here which activates and then deactivates the channel providing a scope to study the path of activation and then the recovery path from inactivation to resting state during refractory period. Using these voltage protocols and nonequilibrium response properties we have characterized the inactivation path both kinetically and thermodynamically which has not been studied earlier. In this respect we are mainly interested here to understand the dynamical mechanism of inactivation in contrast to the molecular mechanism which are traditionally searched for. More specifically using the model of Vandenberg and Bezanilla[33] for various protocols here we have explored the following queries regarding sodium ion channel inactivation:

1. How the channel does react to the constant voltage protocol and what is the favored path of inactivation in terms of CSI and OSI?
2. What is the preferred path of inactivation during test pulse and base pulses of pulse train protocol and continuously oscillating voltage protocol?
3. How does the non-equilibrium thermodynamic quantities like total entropy production rate contribute to the kinetic understanding?
4. How do these different voltage protocols collectively contribute toward our general understanding of inactivation path or how the different response natures toward different protocols enlighten the mechanism of channels inactivation path?
5. How the channel's inactivation path does get modified in presence of drugs?

Kinetic scheme of sodium ion channel

To describe the kinetics of the Na^+ ion channel, here we have used the familiar 9 state model proposed by Vandenberg and Bezanilla.[33] In this proposed model we have considered the data of human cardiac isoform(hH1a)[27] of the sodium channel or Nav 1.5. In the Figure 1 we have shown the model. Here it's worth mentioning the reason why we have chosen this model. Comparing the 2 well known models of sodium channel, namely Vandenberg-Bezanilla[33] and Millonas-Hanck[27] model, for the same system(i.e, human cardiac isoform, hH1a) Kargol[30] showed that both the models fit with the experimental data for the stepped-potential protocols equally well. For custom designed fluctuating voltage pulses that drives the protein molecule far from its equilibrium state, both the models almost equally fit the experimental data.[30] Therefore we selected this model for studying non-equilibrium response using time dependent voltage protocols.

At the resting potential (−70 mV) the most preferred state is P_0. After depolarization, several sequential steps occur i.e., transition from P_1 to P_4 occurs corresponding to the different conformational states of the protein involved(attributed to the gradual

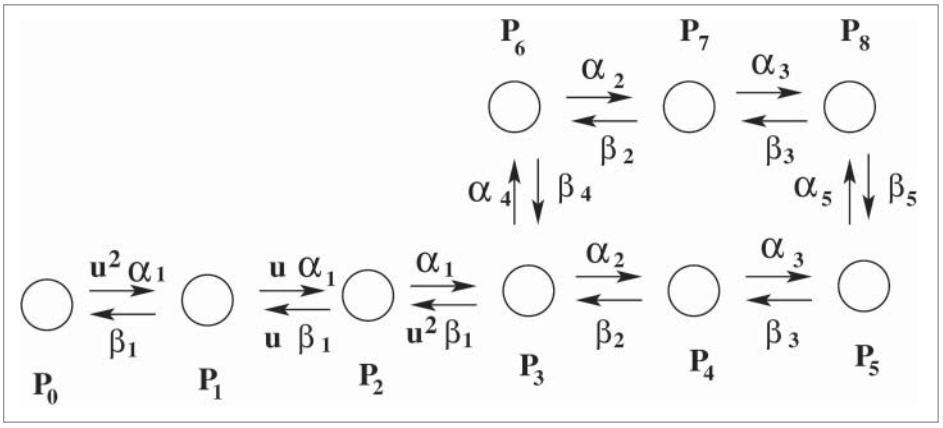

Figure 1. Kinetic model. Experimentally fitted sodium ion channel model of Vandenberg *et. al.*[33] P_0 is the resting state. P_1 to P_4 are closed states. As soon as the stimulus comes several sequential transitions from P_0 starts and finally goes to open-state, P_5. After that the channel goes to inactivated state as described by P_6, P_7, and P_8 states.

activation of all 4 domains of the protein, D-I to D-IV) are required to finally open the pore to allow influx of sodium ions, resulting in macroscopic ionic current. The single ion conducting or open-state is represented by P_5. P_1 to P_4 are closed states. The next important step observed in sodium channel is inactivation. As soon as the cell depolarization reaches a certain critical value sodium channel automatically inactivates to stop further in-fluxing of sodium ions into the cell which leads to the fall in magnitude of sodium ionic current, I (t). P_6, P_7 and P_8 are the inactivated states in this model. As soon as the inactivation occurs the work of sodium channel is finished for now and remains in this inactivated state until the re-polarization of the cell is completed by potassium channel. The forward and backward transition rates are $\alpha_i(V(t))$ and $\beta_i(V(t))$, respectively which are voltage dependent. The functional forms of the rate constants are given by,

$$\alpha_i(V(t)) = \alpha_i(0)e^{\frac{q_i\, eV(t)\delta_i}{k_B\, T}} \text{ and } \beta_i(V(t)) = \beta_i(0)e^{\frac{-q_i\, eV(t)(1-\delta_i)}{k_B\, T}}. \tag{1}$$

Here $q_i^{\pm}$ are the gating charge involved with each forward and backward transitions, respectively. $\alpha_i(0)$ and $\beta_i(0)$ represent the forward and backward transitions, respectively at zero voltage. T is the absolute temperature with $\frac{k_B T}{e} = 24.4$ mV, δ_i = fractional electrical distance ($0 < \delta_i < 1$), a dimensionless parameter and u = 1.2 is a fitting parameter. The parameters associated with these 9 coupled differential equations are given in the following Table 1.

Parameter, $\alpha_4(V) = \frac{\alpha_4(V)\beta_5(V)}{\beta_5(V)}$, is a constraint to maintain microscopic reversibility. The total gating charge of the model is 11.8 e. The time evolution of the probabilities of the 9 states can be written in terms of 2 general master equations. For convenience we have considered two indices, "A" and "I" which represent the active states (P_0 to P_5) and inactive states (P_6 to P_8), respectively. The master equation corresponding to the active state can be written as:

$$\begin{aligned}\frac{dP_A(i,t)}{dt} &= w^{+}_{(i-1)}\Big(V(t)\Big)P_A(i-1,t) \\ &+ w^{-}_{(i+1)}\Big(V(t)\Big)P_A(i+1,t) - w^{+}_{(i)}\Big(V(t)\Big)P_A(i,t) \\ &- w^{-}_{(i)}\Big(V(t)\Big)P_A(i,t) + \delta_{3,i}[-l_1\Big(V(t)\Big)P_A(i,t) \\ &+ l_{-1}\Big(V(t)\Big)P_I(2i,t)] + \delta_{5,i}[-l_2\Big(V(t)\Big)P_A(i,t) \\ &+ l_{-2}\Big(V(t)\Big)P_I(i+3,t)],\end{aligned} \tag{2}$$

where $P_A(i, t)$ represents the probability of remaining in the i-th active state at time t. Similar sort of

Table 1. Model parameters are taken from Millonas et al. 1998.

Rate index	α_i (0)(s^{-1})	β_i (0) (s^{-1})	q_i	δ_i
1	4779	10.3	2.83	0.053
2	5045	12.1	3.16	0.5
3	1684	2360	0.077	0.78
4	19.8	$\frac{\alpha_4\,\beta_5}{\alpha_5}$	5.573	0.12
5	800	59.8	0.16	0.33

expression holds for inactive state master equation as

$$\frac{dP_I(i,t)}{dt} = w^{+}_{(i-1)}(V(t))\ P_I(i-1,t) + w^{-}_{(i+1)}(V(t))\ P_I(i+1,t) - w^{+}_{(i)}(V(t))\ P_I(i,t) - w^{-}_{(i)}(V(t))\ P_I(i,t) + \delta_{6,i}\left[l_1(V(t))P_A\left(\frac{i}{2},t\right) - l_{-1}(V(t))P_I(i,t)\right] + \delta_{8,i}[l_2(V(t))P_A(i-3,t) - l_{-2}(V(t))P_I(i+3,t)]. \quad (3)$$

For active states with population $P_A(i, t)$, the value of i ranges from 0 to 5, whereas for inactive states, i = 6, 7 and 8. $w^{+}_{(i)}(V(t))$ and $w^{-}_{(i)}(V(t))$ are designated as the forward and backward transition rates of i-th state. For example, for the state $P_A(3, t)$, the associated rates are $w^{+}_{(2)} = \alpha_1$, $w^{+}_{(3)} = \alpha_2$, $w^{-}_{(4)} = \beta_2$ and $w^{-}_{(3)} = u^2\ \beta_1$ which can be found from the Figure 1 with $l_1 = \alpha_4$, $l_{-1} = \beta_4$, $l_2 = \alpha_5$ and $l_{-2} = \beta_5$. At any instant of time, t the ionic current, I(t) is calculated by the following equation,

$$I(t) = g_0 g_V(V(t) - V_r)P_5, \quad (4)$$

where $g_0 = 0.0169$ is the overall scaling factor representing the cell expression rate. g_V is the instantaneous conductance, fitted by a third order polynomial expressed as $g_{V(t)} = g_0 + g_1 V(t) + g_2(V(t))^2 + g_3(V(t))^3$, where unit of g_V is μS and $g_1 = -8.21 \times 10^{-4}$, $g_2 = -4.72 \times 10^{-6}$, $g_3 = 1.49 \times 10^{-8}$ with $g_0 = 0.0169$ is the overall scaling factor representing the cell expression rate. V_r is the reversal potential of the sodium ion channel, usually 67.0 mV.

Dynamical characterization of inactivation

For the past few decades characterization of inactivation has been an important topic of research. Various models and theories[5,16,17] regarding fast, slow and ultra-slow inactivation[3] have come up. Even though the crystal structure of sodium channel in potentially 2 inactive states[34,35] are found, still the path of inactivation[19] happens to be a matter of debate. Almost all recent studies involve molecular structure related information which are very hard to speculate from theoretical perspective. Besides proper non-equilibrium energetics of inactivation path has never been considered. Also how does the different voltage protocols used in the experiments for characterizing the sodium channel inactivation collectively contribute toward our basic understanding of inactivation path is still not addressed in a general framework. Thus studying the simple kinetic flux analysis and thermodynamic contribution of total entropy production rates associated with these inactivation paths we have characterized the dynamical profiles of CSI and OSI in this paper. Before going to the different voltage protocols used, here we have briefly discussed the kinetics and thermodynamics of inactivation path in the following subsections.

Kinetics of CSI and OSI

There are 2 possible ways of inactivation as seen from in the model. One is from pre-open closed state, i.e. from P_3 to P_6 (CSI, closed state inactivation) and another is from open-state, i.e., from P_5 to P_8 (OSI, open-state inactivation).[21,26] Both of the paths are responsible for inactivation but depending on the kinetic rate parameters and voltage protocols applied we can qualitatively understand here which one is the most favorable path for inactivation, simply by calculating the net flux direction and magnitude. Here we designate the CSI and OSI as follows,

$$\mathrm{CSI}(t) = [\alpha_4\ (V(t))P_3(t) - \beta_4\ (V(t))P_6(t)]$$

and

$$\mathrm{OSI}(t) = [\alpha_5\ (V(t))P_5(t) - \beta_5\ (V(t))P_8(t)]. \quad (5)$$

Nonequilibrium thermodynamic characterization of inactivation path

Next we have studied the non-equilibrium thermodynamic aspect of the inactivation path of sodium channel in terms of the entropy production rates. Here we have considered that the system remains in contact with the environment with temperature, T. We begin with the definition of system entropy[36] as,

$$S_{\mathrm{sys}} = \frac{k_B}{2}\sum_{i,j} P_i(t)\ln P_i(t), \quad (6)$$

where k_B is the Boltzmann constant. The system entropy production rate (epr) is calculated to obtain

the following expression,

$$\dot{S}_{\rm sys}(t) = \frac{k_B}{2}\sum_{i,j}\left[q_{ij}(V(t))P_i(t) - q_{ji}(V(t))P_j(t)\right] \times \ln\left[\frac{P_i(t)}{P_j(t)}\right]. \quad (7)$$

Here q_{ij} is the transition rate which converts the state from i to j. Similarly reverse transition occurs for q_{ji}. Now the system epr[37,38] is defined as,

$$\dot{S}_{\rm sys}(\mathrm{t}) = \dot{S}_{\rm tot}(\mathrm{t}) - \dot{S}_{\rm med}(\mathrm{t}), \quad (8)$$

where is $\dot{S}_{\rm tot}$ (t) total epr and $\dot{S}_{\rm med}$ (t) is the medium epr, appearing due to entropy flux into the surroundings[39,40] as follows,

$$\dot{S}_{\rm tot}(\mathrm{t}) = \frac{k_B}{2}\sum_{i,j}\left[q_{ij}(V(t))P_i(t) - q_{ji}(V(t))P_j(t)\right] \times \ln\left[\frac{q_{ij}(V(t))P_i(t)}{q_{ji}(V(t))P_j(t)}\right], \quad (9)$$

and

$$\dot{S}_{\rm med}(\mathrm{t}) = \frac{k_B}{2}\sum_{i,j}\left[q_{ij}(V(t))P_i(t) - q_{ji}(V(t))P_j(t)\right] \times \ln\left[\frac{q_{ij}(V(t))}{q_{ji}(V(t))}\right]. \quad (10)$$

Now, for the constant voltage case all the transition rates associated with these eprs are time independent and for pulsed and oscillating voltage case they are functions of both voltage and time. In addition one should note that when detailed balance holds the total epr vanishes i.e., $\dot{S}_{\rm tot} = 0$, as $q_{ij}P_i(t) = q_{ji}P_j(t)$, which is clearly a case of equilibrium situation where all other eprs are also zero. On the contrary when $\dot{S}_{\rm tot} > 0$, it should go to a non-equilibrium steady state which demands the situation of broken detailed balance, i.e. $q_{ij}P_i(t) \neq q_{ji}P_j(t)$.

Now we shall be concentrating on the total entropy production rates associated with the CSI and OSI paths. Thus the total entropy production rate of the CSI path is written as,

$$\dot{S}^{\rm CSI}_{\rm tot}(t) = \frac{k_B}{2}\sum_{i,j}\left[\alpha_4(V(t))P_3(t) - \beta_4(V(t))P_6(t)\right] \times \ln\left[\frac{\alpha_4(V(t))P_3(t)}{\beta_4(V(t))P_6(t)}\right]. \quad (11)$$

Similarly for open-state inactivation path the total entropy production rates associated can be written as,

$$\dot{S}^{\rm OSI}_{\rm tot}(t) = \frac{k_B}{2}\sum_{i,j}\left[\alpha_5(V(t))P_5(t) - \beta_5(V(t))P_8(t)\right] \times \ln\left[\frac{\alpha_5(V(t))P_5(t)}{\beta_5(V(t))P_8(t)}\right] \quad (12)$$

Next we have defined here quantities such as F-CSI and F-OSI which are the percentages of the total epr associated with the closed-state inactivation path and open-state inactivation path, respectively. These quantities are given as follows.

$$\mathrm{F-CSI\,(\%)} = \frac{\dot{S}^{\rm CSI}_{\rm tot}(t)}{\dot{S}_{\rm tot}(t)} \times 100,$$

and

$$\mathrm{F\text{-}OSI\,(\%)} = \frac{\dot{S}^{\rm OSI}_{\rm tot}(t)}{\dot{S}_{\rm tot}(t)} \times 100. \quad (13)$$

These nonequilibrium thermodynamic quantities like total entropy production rates provide the information about the entropic cost associated with these 2 paths. The CSI-epr and OSI-epr actually shows the dissipation of energy via these 2 paths. A path which is more dissipative is more favored by the system. The CSI-epr and OSI-epr actually shows which path is more favorable during various depolarizations.

Constant voltage protocol

Generally the constant voltage clamp technique is used by electrophysiologists to measure the ionic current through the membrane of excitable cells, while holding the membrane voltage at a set level. The voltage clamp allows the membrane voltage to be manipulated independently of the ionic current, allowing it to study the current-voltage relationship of the voltage gated sodium channel. For the constant voltage case the transition rates become time independent as the

voltage is kept constant throughout the time course of the study. Before we start characterizing the inactivation we have studied the ionic currents, probabilities at different voltages numerically. We have used Runge-Kutta algorithm for solving 9 coupled differential equations here. All the rate constants and the parameters are already given in the section of kinetic scheme.

From the Figure 2A it is seen that with the onset of depolarization ionic current initially increases, allowing influx of sodium ion current inside the cell membrane, and after passing through a maxima (maxima, because, I(t) = -ve, the more negative, the more influx of current into the cell) ionic current decreases. Generally the first part of increasing ionic current is called the activation and the decreasing part of ionic current is called inactivation. From Figure 2B it is observed that open-state probability P_5 gradually decreases and the inactive states start rapidly and takes higher values than P_0 to P_5 states, inferring that the system ultimately goes to inactivated state.

In Figure 2C we have plotted the total epr with time for −45, −30 and +15 mV. For all the voltages it is seen that the system quickly attains the equilibrium as seen from vanishing total epr.[41] For the constant depolarization system always adjust itself with it and equilibrate finally. With the increase in depolarization, system goes to equilibrium in a faster rate. Now as details balance holds in equilibrium with all opposite fluxes are balanced by each other, thereby CSI and OSI also vanish. For this reason if we want to study the paths of inactivation in terms of CSI and OSI, we have to keep the system driven or out of equilibrium by applying some external time dependent voltage protocol, as discussed in the next 2 sections.

Activation and inactivation dominated regions

It is also observed from Figure 2A that with the increasing depolarization inactivation occurs in a faster rate. As the activation and inactivation process occurs simultaneously it is hard to differentiate this to process as they are mutually coupled to each other. We can at least find the region of voltages where the activation process predominates and vice versa. So, if we calculate the net amount of ionic current in-fluxed into the cell by calculating the area under the curve of ionic currents in various depolarizations, up to their respective steady-states, we must observe a region of voltage in which the channel will allow more and more current with more depolarizations. After a certain value of depolarization the channel will close with much faster rate, inhibiting ion influx. The integrated ionic current stated above is calculated as

$$\mathrm{I_{Area}} = \int_0^{t_s} I(t)dt, \tag{14}$$

where t_s is the time to achieve the steady state for a certain voltage. t_s changes as voltage changes. As the voltage increases from -ve region to +ve region the t_s decreases. In Figure 2D, $\mathrm{I_{Area}}$ is plotted against various depolarizations. From this figure it is observed that up to ∼ −70 mV there was no current influx as −70 mV is the resting potential of the cell. Above ∼ −70 mV,

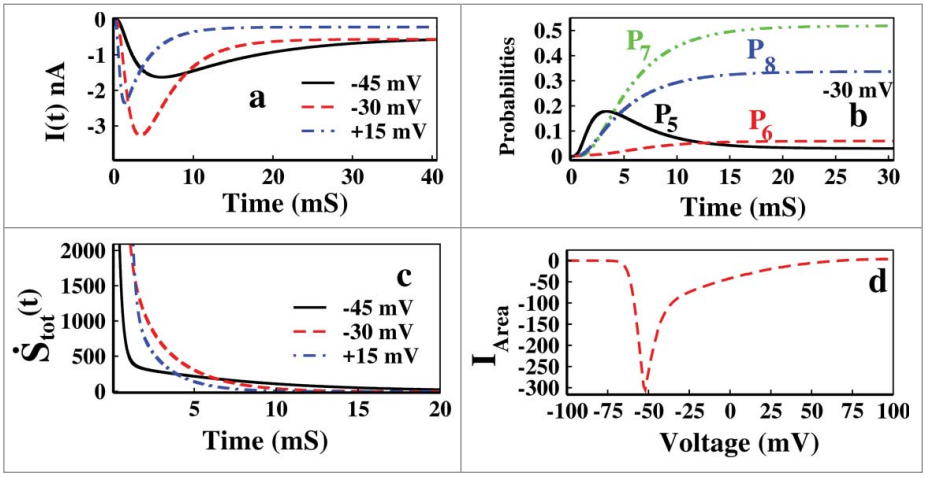

Figure 2. Characterization of inactivation at constant voltage. In (A) ionic current at constant values of depolarization such as −45, −30, +15 mV are shown. In (B) open-state, P_5 and inactive states, P_6, P_7, P_8 probabilities with time at a depolarization of −30 mV is shown and in (C) total epr, $\dot{S}_{tot}(t)$ vs. time has been plotted for −45, −30 and +15 mV, respectively. In (D) the integrated ionic current vs. various depolarization up to their steady state points, t_s have been shown.

the integrated ionic current, I_{Area} increases and that is why it is called as the activation dominated region (−70 to −50 mV). After that the integrated ionic current decreases and so the rest of the part is inactivation dominated region. Given the rate constants the ranges of these domains vary in different sodium channels.

Choice of voltage region to study inactivation

Choice of voltage region to study inactivation is one of the important task we have to do in constant voltage protocol. To extract information about inactivation it is instructive to study the system in a voltage region where inactivation predominates, especially for the model oriented studies, where activation phenomena can affect the inactivation less. Beside the kinetic model and rate parameters also determine the region where one should study the model for inactivation. In our model we have found that for constant voltage case, it is worth studying inactivation above −55 mV. In the Figure 3 we have plotted the sum of the probabilities of all 3 inactive states, ($P_6 + P_7 + P_8$) along with the 3 resting states, ($P_0 + P_1 + P_2$). From the curves we can see that the channel actually gains probability of attaining inactivated state above −55 mV, below which the probability of remaining in the resting states is very high or the system hardly activates. Thus for constant voltage protocol it is worth studying the system above −55 mV where the channel has maximum probability of attaining inactivation. Once again we want to mention that this voltage region varies from model to model and with associated rate parameters. Thus for the next analysis regarding the inactivation, we have applied the voltage starting from −55 mV to above.

Waiting time analysis of inactive states

To characterize the inactivation process we want to study the mean waiting time for inactivation in different voltages. The inverse of this quantity shows an approximate rate of inactivation. Now we calculate the mean waiting time as follows,

$$\langle t_{wt}^{in} \rangle = \int_0^{t_s} t. \frac{d(P_6 + P_7 + P_8)}{dt} dt, \qquad (15)$$

where we calculate the mean waiting time of overall inactivation including all the inactive states such as P_6, P_7 and P_8. Then we plot the mean waiting time as a function of voltage.

In Figure 4A and B, the mean waiting time has been plotted for various depolarizations. It is seen that from −50 mV the mean waiting time gradually decreases with increasing depolarization. As with increasing

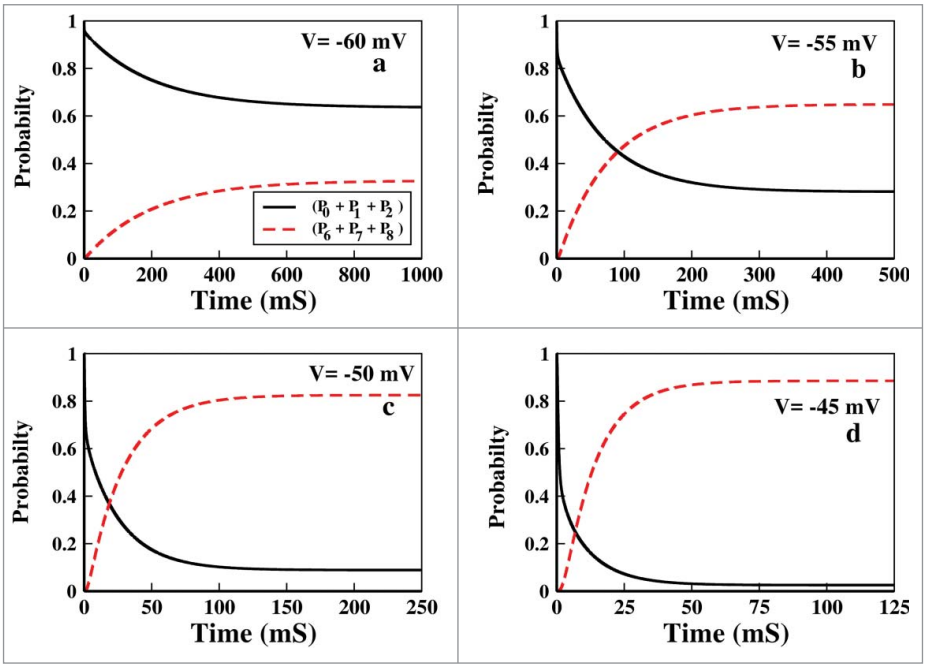

Figure 3. Choice of voltage range. In (A to D) The collective probability of the resting states(see text) and the inactive states have been plotted for voltage −60, −55, −50 and −45 mV, respectively.

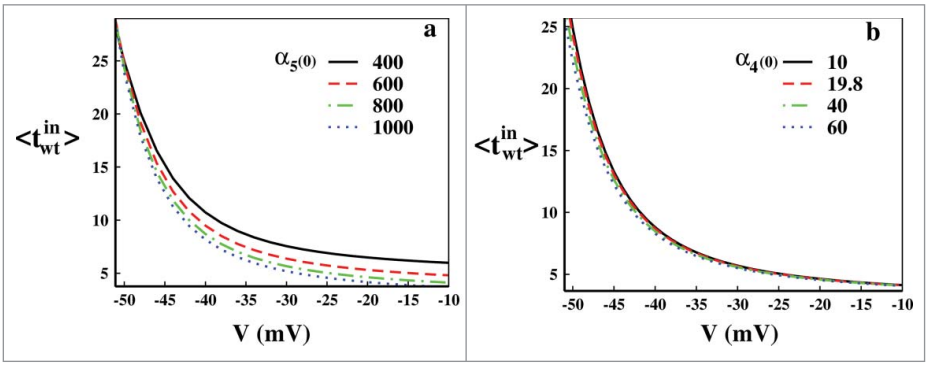

Figure 4. Waiting time analysis. In (A) waiting time analysis at different voltages with $\alpha_5(0) = 1000$, 800(original), 600 and 400 have been plotted up to their steady-states. In (B) similar waiting time analysis is done for $\alpha_4(0) = 60$, 40, 19.8(original) and 10.

depolarization inactivation occurs with faster rate the mean waiting time decreases. This result is also consistent with the result of Figure 2C.

As we are interested in the inactivation path, next we have shown the effect of change in the rate constants associated with the CSI and OSI paths. The change of rate constants can be physically attributed to the mutation originated disorders. Various mutations and hereditary diseases can change the rates of the path of inactivation. Here we have changed the rate constants α_5 and α_4 to observe the effect in mean waiting time associated with OSI and CSI, respectively. In Figure 4A we have varied the $\alpha_5(0)$ from 400 to 1000 s^{-1}, where green dot-dashed line with 800 s^{-1} is the original rate constant as mentioned in Table 1. Similar plots have been done for Figure 4B for $\alpha_4(0)$ from 10 to 60 s^{-1}. It is quite expected that with increasing rate constants, the mean waiting time should decrease as the rate of inactivation increases. This is also evident from Figure 4A and B. It is worth mentioning that the change in the rate constants of CSI path do not affect the mean waiting time or rate to a considerable amount. But the change in the rate constant of OSI path affects the overall rate of inactivation considerably which intern also concludes that the OSI path of inactivation occurs in a much greater extent than CSI in this voltage region.

Constant voltage inactivation path

Now we have come to our desired goal of characterization of the inactivation path in constant voltage protocol. Here we have observed the total amount of flux associated with the closed-state inactivation and open-state inactivation. Thus we have calculated the following quantities, which provide the net amount of CSI and OSI occurred in a certain voltage up to the respective steady-state.

$$A_{\mathrm{CSI}} = \int_0^{t_s} \mathrm{CSI}(t)\ dt \text{ and } A_{\mathrm{OSI}} = \int_0^{t_s} \mathrm{OSI}(t)\ dt. \tag{16}$$

The definitions of CSI and OSI have been taken from equation (5). In Figure 5A and B A_{CSI} and A_{OSI} are plotted. It is seen that the net amount of CSI is lesser than the OSI for all voltages. Also it is seen that with increasing depolarization the amount of CSI decreases but OSI increases. Thus it is observed that in this region of depolarization OSI is the most preferred path of inactivation. In general most of the sodium channels use both CSI and OSI. However some channels undergo more inactivation from the open-state and others undergo more inactivation from CSI. These distinct behaviors can be classified as preferential OSI and preferential CSI.[21] The results here in this paper show that our system is a preferential OSI system.

Pulse train protocol

The pulse train protocol is a popular and a very powerful nonequilibrium spectroscopic tool to study the channel gating process, inactivation procedure and recovery from inactivation.[42-45] Here we want to investigate the path of inactivation in presence of consecutive test pulses and base pulses. The pulse train is applied in the following manner. First, a base pulse of −80 mV is provided to the system for few milliseconds and then test pulse train of −45 mV is initiated. Each

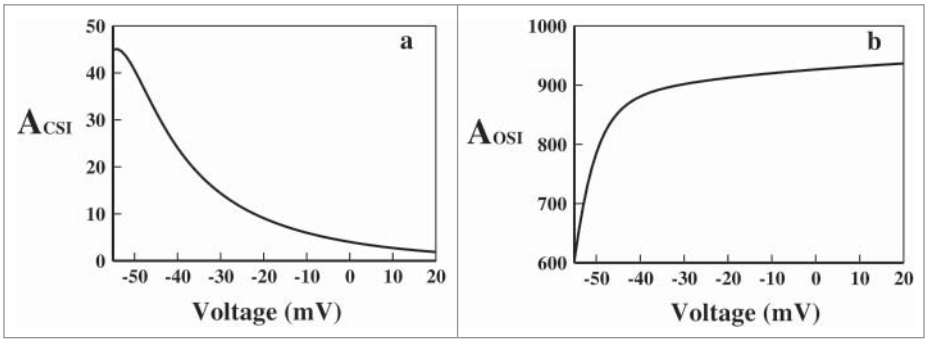

Figure 5. Path of inactivation in constant voltage protocol. In (A) the A_{CSI} (see text) and in (B) the A_{OSI} (see text) are plotted for various voltages, respectively.

test pulse in the pulse train is brought back to −80mV base voltage and then again fired to test voltage. The applied pulse train is shown in Figure 6A. This important nonequilibrium spectroscopic tool replicates the real biological situation where sodium channel responds to a repetitive stimulus. Here the −45mV test pulse activates the system and the base pulse causes necessary refractory changes to the system to prepare it ready for the next incoming pulse. An interesting advantage of using pulse train protocol is that we can actually control the population of various states as desired. As for example the test pulse of −45mV will populate the open-state and inactive states while the base pulse will again depopulate them and will populate the resting state. While populating the resting states, it will provide us a scope to identify the path of re-factorization to the resting state, which has been a major part of investigation.[25] In Figure 6B the corresponding ionic current is shown. It is seen that after the first pulse the peak of the ionic current is gradually reduced as seen in the experiments done earlier.[44]

For our purpose of characterization of the inactivation path we concentrate on the first 200 ms of the pulse train and for studying the kinetic and the thermodynamic contribution of the closed- state and open-state inactivation. It enables us to understand

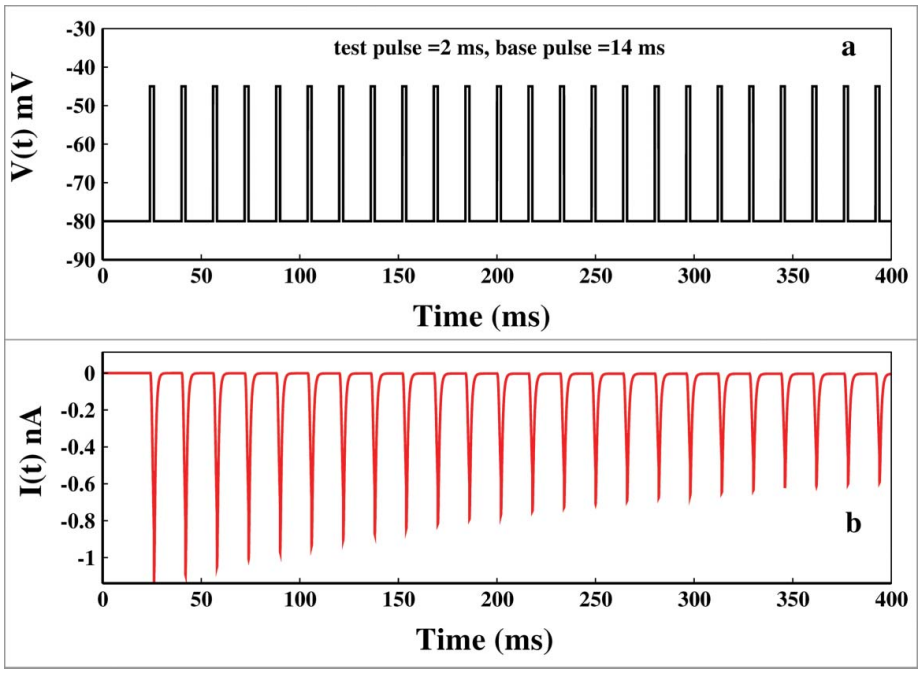

Figure 6. Pulse train protocol. In (A) at first the voltage is kept at −45 mV and after few milliseconds it is brought back to base −80 mV after that the pulse train begins. Here the base pulse duration is 14 ms and test pulse duration is 2 ms. In (B) the corresponding ionic current is plotted.

which path is more favored during test pulse and during refactoring base pulse.

Kinetics of CSI and OSI in pulse train protocol

Here we designate the forward flux of CSI path as CsF and the backward flux as CsB. They are expressed as CsF = α_4 P_3 and CsB = β_4 P_6. Similarly for OSI path, OsF = α_5 P_5 and OsB = β_5 P_8.

Now comparing the Figures 7B and F it is clearly seen that during the test pulses the net OSI is almost 10 times of the magnitude of the net CSI and also the magnitude of the OSI is +ve, indicating that during the test pulse the open-state inactivation path is preferred. The magnitude of CSI is 10 times lesser than OSI indicating very small probability of occurring inactivation through CSI path. Also it is seen that the magnitude of the CSI and OSI during the test pulses is gradually decreasing. Thus with time both types of inactivation gradually decreases down. One thing we have noticed that the CSI during base pulses gradually becomes more negative after each pulses as seen from the inset of Figure 7B but the OSI remains almost zero during base pulses for all the time. Now to understand the increasing negative magnitude of CSI and the nature of OSI which is almost zero all the time during base pulses, we need to look at the forward and backward fluxes associated with these paths.

Now as we defined CSI=(CsF - CsB) and OSI=(OsF - OsB), if CSI is +ve then the path P_3 to P_6 is followed. Again if CSI is -ve, then the path P_6 to P_3 is followed and similarly for OSI path. Now comparing the Figures 7C and G it is seen that during the *test pulse* CsF is almost 10 times lesser than OsF. Thus closed-state inactivation during test pulse also occurs along with open-state inactivation but with negligibly less amount. During the test pulse the OsF is the most favored path. It is worth mentioning that in Figure 7H the OsB flux is seen to be gradually increasing. It is just a mathematical interpretation of the fact that the inactive states are gradually populating or the channel's inactivation via open-state is gradually decreasing. It does not mean that the system reverts back from inactive state to open-state, which is not true in real situation. To hold the microscopic reversibility each Markov model has forward and backward rates.

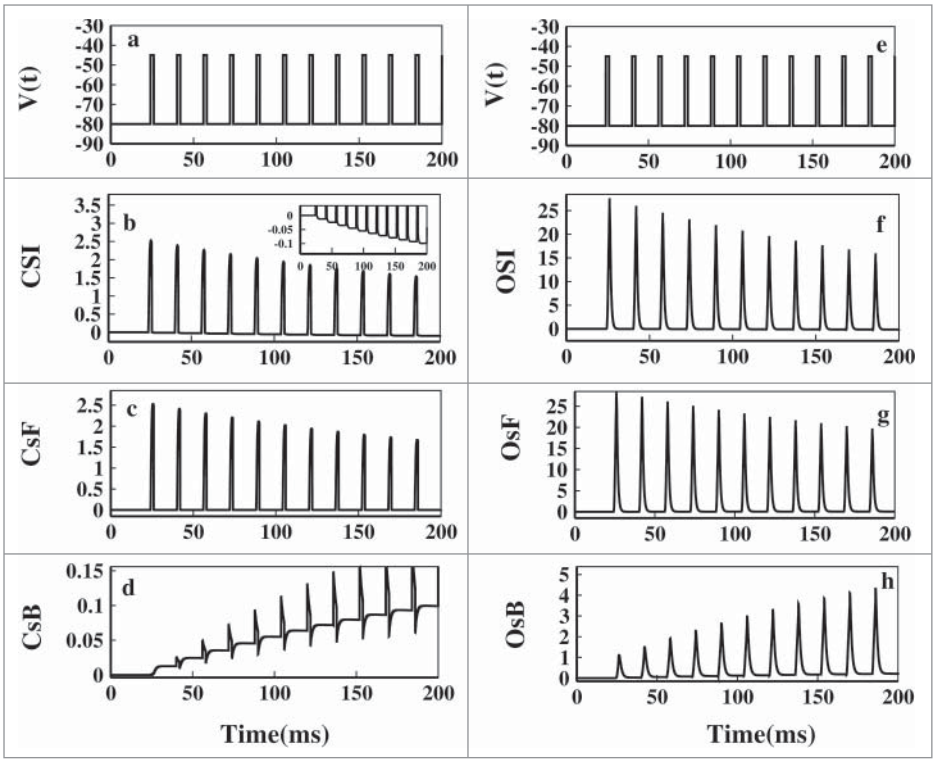

Figure 7. Pulse train fluxes. The left panel(A-D) corresponds to the fluxes of closed-state inactivation(CSI) and the right panel(E-H) corresponds to the open-state inactivation(OSI) path. In (A) and (E) the selected first 200ms pulses of Figure 6A has been plotted. In (B) and (F) net CSI and net OSI has been plotted respectively. In (C) and (G) forward flux(CsF) of CSI path and forward flux(OsF) of OSI path are plotted respectively. In (D) and (H) backward flux(CsB) of CSI path and backward flux(OsB) of OSI path are plotted, respectively. The inset figure of (B) shows the gradual increase of negativity of CSI during base pulses.

It is thus always instructive to study the net flux which is OSI/CSI instead of giving much of emphasis on individual fluxes, especially for the model oriented kinetic study. Studying individual fluxes are necessary for detailed theoretical understanding of the dynamics of the system but sometimes in reality they are more or less irreversible.

Now an interesting feature is seen in the base pulses. During the *base pulses* CsF is close to zero but the CsB is -ve and the negativity gradually increases with time with each base pulse as seen from Figure 7D making the CSI more and more -ve during base pulses as seen in Figure 7B(inset). Here OsF and OsB are approximately zero, indicating that during repolarisation the OSI fluxes has almost no contribution to the system dynamics. This clearly says that during the base pulses the system reverts back to resting state via closed state via CsF path. Shab K^{+}[46] channels and most of the sodium channels bypasses the open-state during recovery from inactivation.[47] Our analysis certainly agrees with that. Also the rate of recovery from inactivation increases after each pulse with increase in the inactive states population.[44] Thus we have the following situation during the test pulse and base pulse as seen in Figure 8.

5.2. Non-equilibrium thermodynamics of CSI and OSI in pulse train protocol

In Figure 9 we have plotted the time dependent entropy production rates for pulses starting from 0 ms to 300 ms. From Figure 9B it is seen that the total entropy production rates shows sharp peaks instantly after onset of both test pulses and base pulses. But the peak height gradually decreases down. With the onset of test or base pulses system goes far from the equilibrium as seen by the non-zero values of the dissipation function or the total epr at the peaks. Any change in the depolarization instantly changes the state of the system. Here we want to mention that within this 2 ms test pulse duration the system cannot reach the equilibrium and also during the 14 ms base pulse duration system does not achieve the equilibrium but remains very close to it. These durations are purposefully set so small so that we can study the relaxation or the response dynamics in nonequilibrium environment.

In this situation, we have seen the entropic contributions arising due to closed-state inactivation and open-state inactivation. From the Figures 9C we can see that the entropic contribution of CSI path during the test pulses gradually decreases down. Also during the test pulse $\dot{S}_{tot}^{OSI}(t)$ has significantly higher magnitude than the $\dot{S}_{tot}^{CSI}(t)$ as seen from Figure 9D. Oppositely during the base pulse the CSI contribution gradually increases as seen from of the inset of Figure 9C but $S_{tot}^{OSI}(t)$ remains zero all the time during base pulses. As the population of inactive states increase with each test pulse, re-factorization entropy production rate increases with each base pulses. From this thermodynamic analysis we can conclude in correspondence with the kinetic analysis done earlier that during the test pulse OSI path is favored and during base pulse CSI path is favored. The Figures 9E shows

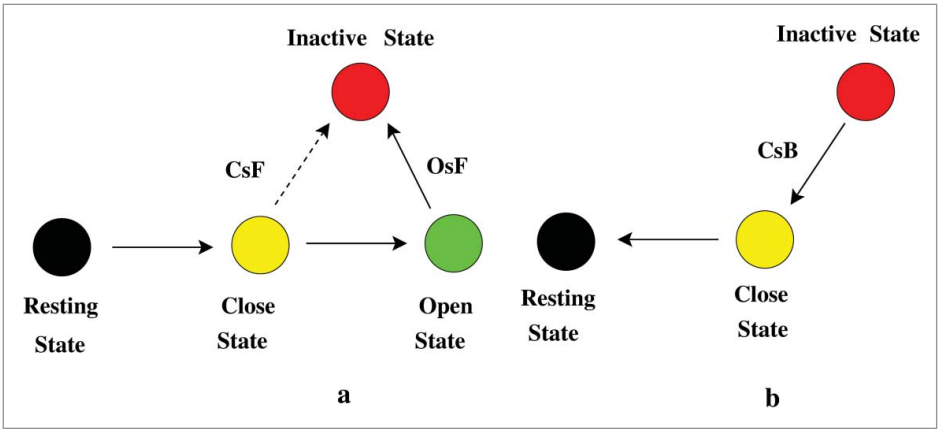

Figure 8. Path during activation and recovery from inactivation. In (A) the test pulse path of inactivation has been shown. During the test pulse the system from resting state P_0 goes to closed-state P_3 to P_5 and then via OsF path goes to inactivation. There is a small probability of occurring inactivation via CsF path. The bold solid arrow line indicates the most preferred path of inactivation, OsF. In (B) the recovery from inactivation or refractory path during base pulse is shown. During the base pulse the system from inactivated state goes to resting state via CsB path.

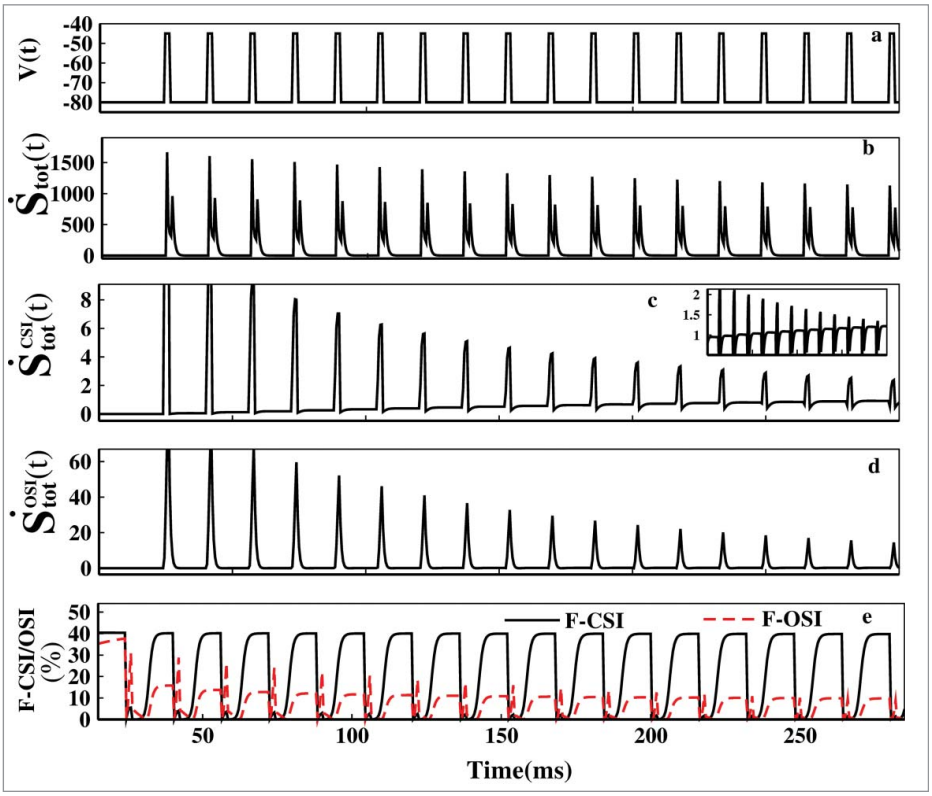

Figure 9. Non-equilibrium dissipation. In (A) the pulse train is shown for the first 300 ms. In (B) $\dot{S}$ tot(t) is plotted. In (C) S^{CSI}_{tot}(t) and in (D) S^{OSI}_{tot}(t) has been plotted. The F-CSI (%) and F-OSI (%) is plotted in (E).

the percentage of CSI and OSI contributions of total entropy production rate, respectively. Here in both the graphs the responses are slightly left sifted due to the complex natures of the F-CSI and F-CSI functions. But the general trend is similar to the kinetic trend with more clarity now i.e., during the depolarization OSI fraction of the total epr is greater than CSI. But during the repolarization the CSI fraction is greater than OSI. With each test pulse the OSI fraction gradually decreases down.

Oscillating voltage protocol

Oscillating voltage protocol is an emerging technique to study the ion channels in non-equilibrium environment.[27,29] In individual neuron the oscillation may appear due to the oscillating nature of action potential and membrane depolarization. Here we have theoretically studied the kinetic as well the thermodynamic response properties of Na^+ channel by considering the sinusoidal oscillating voltage protocol. Here the sinusoidal external voltage that we apply is expressed as, $V(t) = V_0 + A \sin(\omega t)$, where $V_0 = -70$ mV is the mean voltage around which it oscillates as well as is the resting potential of the neuron, A is the amplitude of the oscillation and ω is the frequency as shown in Figure 9A. To get more biophysical insight we have taken the amplitude of the oscillating voltage, A = 45 mV which covers the entire biological range of activation and inactivation depolarization of sodium channel, i.e. (−115 to −25 mV). By taking these parameters, we have studied the kinetic and thermodynamic response at steady state in one complete cycle of the oscillating voltage. Here the transition rates are time as well as voltage dependent. The idea is to study the inactivation paths and their thermodynamic contributions to the total epr.

In Figure 10A the ionic current is plotted at frequency 50 Hz. The ionic current initially oscillates with larger amplitude and then gradually amplitude decreases and it attains a time periodic steady value. Similarly the total epr finally attains a time periodic steady value. As the total epr is always greater than zero, the system is always out of equilibrium and the steady-state is a nonequilibrium steady state(NESS) or dynamic steady-state.[48] At NESS we have studied the directions of the fluxes to understand the OSI and CSI and their contribution to total epr.

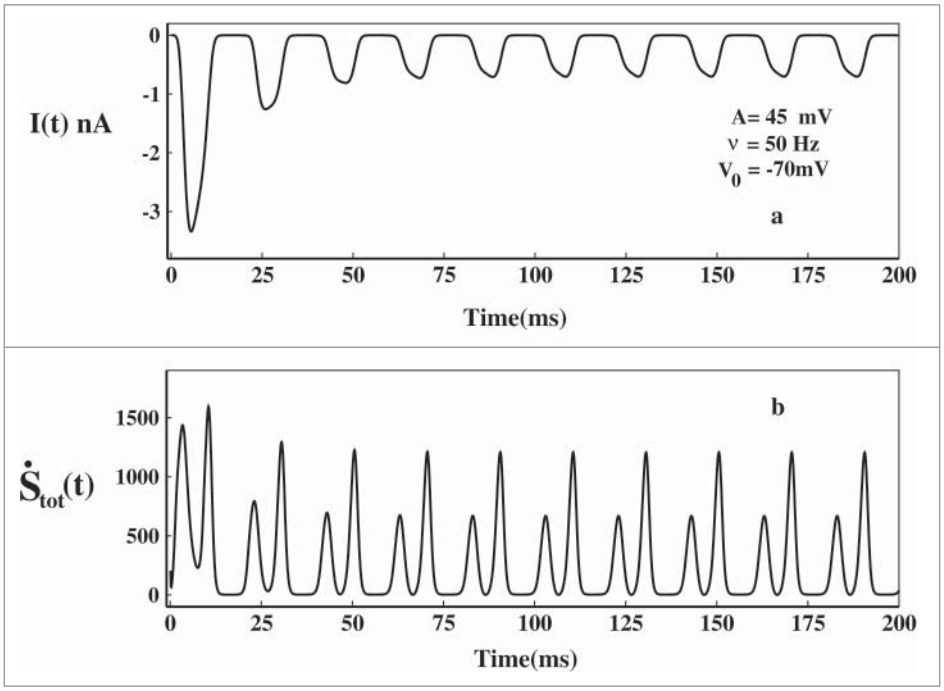

Figure 10. Ionic current and total epr in oscillating voltage protocol. In (A) the ionic current and in (B) the corresponding total epr has been plotted.

Kinetics of CSI and OSI in oscillating voltage protocol

In the Figure 11A and B the voltage of the last oscillation or the NESS voltage variation are shown with time. In Figure 11C and D the CSI and the OSI has been plotted, respectively. It is seen that in the first half of the cycle where the voltage is more depolarizing, i.e., (−70 to −25) mV, the magnitude of the OSI

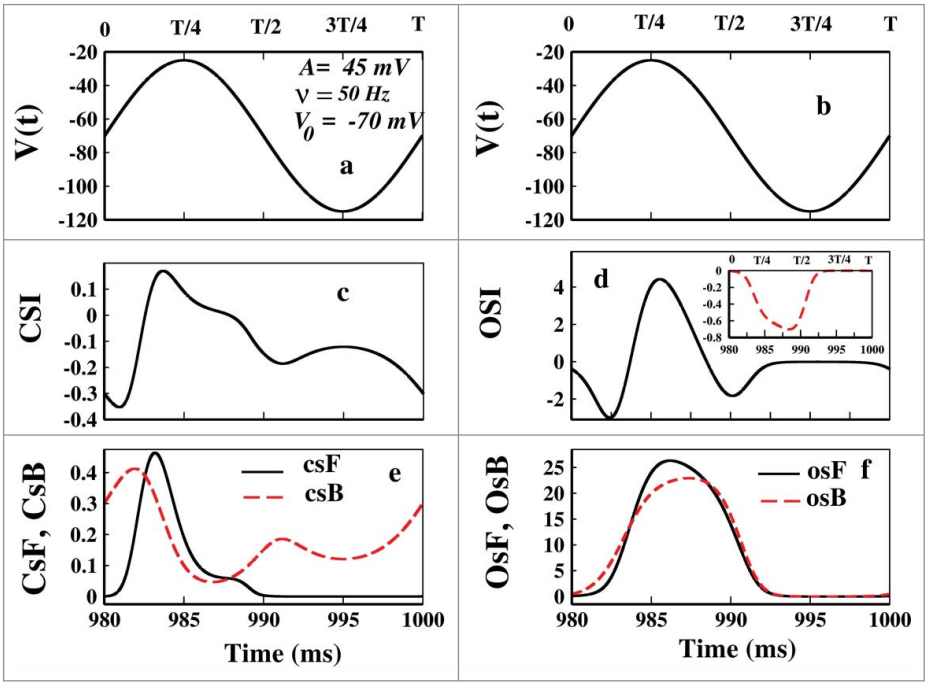

Figure 11. Flux analysis at NESS in oscillating voltage protocol. In (A) and (B) the NESS voltage variation for a cycle has been plotted. In (C) and (D) CSI and OSI have been plotted. The inset shows the ionic current at NESS. It shows that the first T/8 time is electrically silent. In (E) CsF and CsB and in (F) OsF and OsB have been shown.

is much larger than the CSI path. But in the 2nd half when the voltage is in the hyper-polarizing region, i.e. (−70 to −115) mV, the CSI is -ve and OSI is zero almost. This is pretty consistent with the constant and pulse train protocol. It means during the depolarization OSI is more favored than CSI. But during hyper-polarization CSI is favored than OSI.

It is worth mentioning that the negative magnitude at the very beginning of the OSI arising from the kinetic analysis of such kind may infer some phenomenon which does not happen in reality. The negativity of OSI denotes that system from inactive state goes to open-state again. If so then it could not be an electrically silent process[25] then. From the inset of Figure 11E, we can see that the first T/8 ms where OSI is negative is actually electrically silent as it is silent during hyper-polarized region. The negativity of OSI comes from the mathematical construction of the model to maintain the microscopic reversibility which indeed does not show up in the ionic current. This happens because the population of P_8 gradually increases with time. Initially the OsF remains greater than OsB. As the time passes the population of inactive states increases such that at NESS $P_8 >> P_5$, but the forward and backward fluxes becomes comparable. The case of oscillating voltage is somewhat different from the pulsed train. As it is a continuous voltage change, so the system shows somewhat continuity in responses at the beginning or in the end of the each oscillating pulse. It does not change suddenly. However, recovery from inactivation on sodium channel using oscillating voltage protocol still can be a subject of experimental verification as recovery process is a highly voltage dependent.[47] Now from Figure 11E and F it is clear that in the first half of the oscillation OSI is favored than CSI and in the second half CsB is the path during re-polarization, as also seen in pulsed train protocol.

Thermodynamics of CSI and OSI in oscillating voltage protocol

Next we have seen the thermodynamic contribution of CSI and OSI path. In the left panel of Figure 12 the eprs are plotted with time and in the right panel the eprs are plotted with voltage. The total epr of

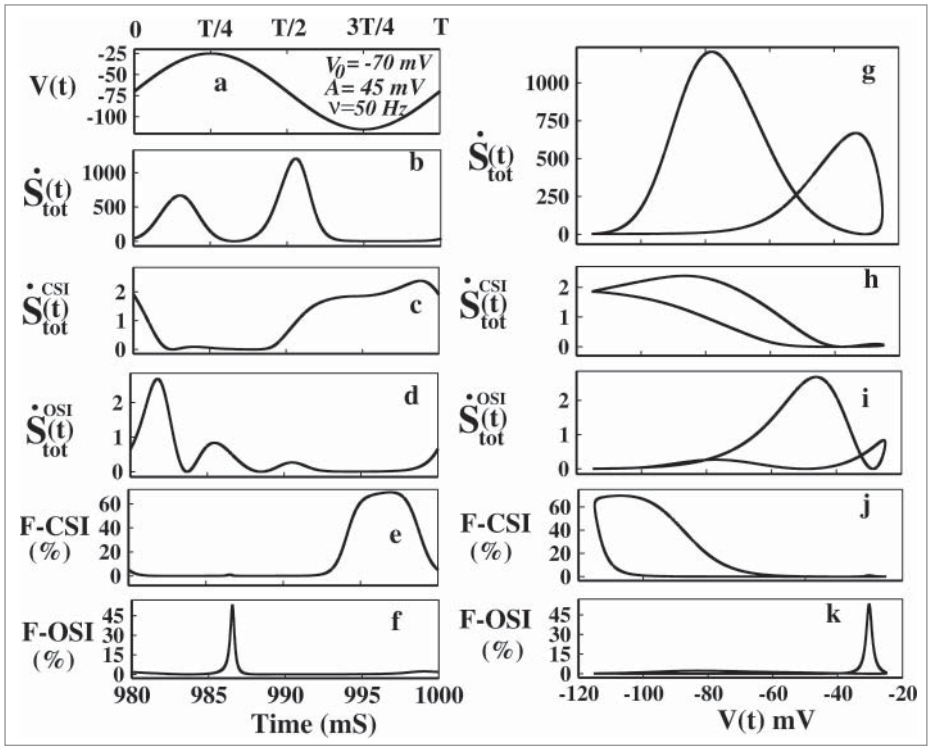

Figure 12. Entropy production rate contributions at NESS in oscillating voltage protocol. In (A) the applied voltage at NESS is shown. In (B) and (G) the total epr with time and voltage has been plotted respectively. In (C) and (H) $\dot{S}_{tot}^{CSI}(t)$ has been plotted with time and voltage respectively and in (D) and (I) $\dot{S}_{tot}^{CSI}(t)$ has been plotted with time and voltage respectively. In (E) and (J) F-CSI (%) has been plotted with time and voltage respectively and in (F) and (K) F-OSI (%) has been plotted with time and voltage, respectively.

the system at NESS is plotted in Figure 12B which shows asymmetric response in the 2 halves of the oscillation. It shows the response is more evident on the left side of the oscillation, i.e., between 0 to T/2. After the T/2 the total epr contribution is negligible, which is correct as in the hyper- polarized region only the CsB path contributes, not all states contributes to the total epr. The total epr is plotted with voltage in Figure 12G which also shows hysteresis property. The kinetic[49] and thermodynamic analysis[41] of dynamic hysteresis of ion channel proves that the ion channel behaves like a memristor device.[50] In Figure 12C the $\dot{S}_{tot}^{CSI}(t)$ is plotted which shows the contribution mainly arises in the second half of the oscillation that is between T/2 to T. In this hyper polarized voltage range (−70 to −115 mV) CSI path shows more contribution than the OSI path as seen after comparing the Figure 12D where the $\dot{S}_{tot}^{OSI}(t)$ mainly contributes to the total epr in the first half of the cycle with more depolarised(−70 to −25mV) voltage case. The F-CSI (%) and F-OSI(%) in Figures 12E and F shows it clearly that the CSI contribution arises in the hyper polarized region while OSI contribution arises in more depolarised region. This behavior is consistent with the pulse train analysis where we have seen that OSI contribution comes in test pulses(depolarizing voltage) and CSI contribution comes in base pulses (hyper-polarizing voltage).

The aforesaid fact is also evident from the right panel figures where the similar quantities have been plotted with voltages. From the Figure 12H it is seen that the loop area of $\dot{S}_{tot}^{CSI}(t)$ is more on the hyper-polarizing voltage region and the loop area of $\dot{S}_{tot}^{OSI}(t)$ is more on the depolarised voltage region as seen from Figure 12I Besides the shape of the hysteresis loop areas of CSI and OSI are clearly distinct to each other. So these 2 paths are also thermodynamically distinguishable or they have distinct thermodynamic signatures. Also we found that the dynamic memory of these 2 paths depends heavily on the frequency and mean voltage, which are not reported here. The fact that OSI occurs in depolarised voltage and refractory changes occur via CSI during hyper-polarization is vivid from the graphs of F-CSI (%) and F-OSI (%) versus voltage in Figure 12J and K, respectively. Thus the thermodynamic analysis very clearly and more efficiently depicts the pathway of activation and re-factorization than kinetic analysis.

Effect of drug in inactivation path

The study of local anesthetics and their binding kinetics to the binding site of sodium ion channel has been important since past few decades.[51-55] In this section we have investigated the effect of drug in the path of inactivation. We have taken a popular example of an open-state drug blocker, Mexilitine[32,55] which mainly attaches to the open- state of the channel and restricts the flow of ions through the channel into the cell. Thus here we add an extra state P_5^M with P_5 for the study of Mexiletine drug binding kinetics[32] as seen from Figure 13. The model is given in Figure 11. We have taken the forward rate constant for binding as $k_{on} = [D] \times 10^5\ s^{-1}$, where [D] is the molar drug concentration [M] and backward rate as $k_{off} = 10^{-2}\ s^{-1}$.[32,56] Both for system under constant voltage and time dependent voltage protocols such as oscillating voltage protocol and pulse train protocol we use

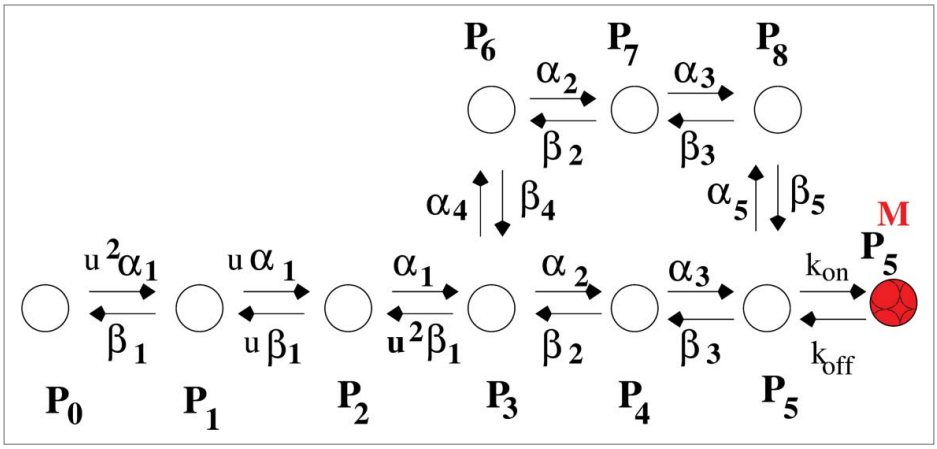

Figure 13. Kinetic model of drug binding. Model of Mexiletine drug blocking is a 10 state model.

these rate constants which are not voltage dependent in any case. Next we have plotted the kinetic effect of drug in open- state inactivation and closed-state inactivation path in presence of constant voltage, pulse train protocol and oscillating voltage protocol. Although this sort of theoretical model oriented studies have limitations[57,58] but it is also true that they can act as useful tools in guiding experimentation[59,60] and may suggest novel directions in studying inactivation.

Effect of drug in constant voltage protocol

In Figure 14A we have shown the effect of Mexilitine in ionic current. It shows with the increase in drug concentrations, ionic current suppresses in a faster rate. Next we have plotted the CSI and OSI for voltages −50, −40 and −30 mV in presence of Mexilitine concentrations such as 0.0001 M, 0.001 M, 0.01 M and 0.1 M. The left panel shows the effect of drug in CSI and the right panel shows the effect on OSI path. From all the CSI curves it is seen that the drug with various concentrations does a little effect on closed-state inactivation path. However the OSI path is greatly affected by the increasing concentration. As the drug has very high binding affinity toward the open-state, inactivation through open- state gradually decreases with increasing drug concentrations.

Effect of drug in pulse train voltage protocol

Here we have showed how the Mexilitine affect the OSI and CSI in presence of pulse train protocol. In Figure 15A the ionic current for the first 300 ms pulse is plotted for 3 different concentrations such as 0.001, 0.01 M. We can see from that figure that with increasing drug concentration the ionic current is decreased gradually. Unlike the constant voltage protocol here in pulse train protocol one interesting phenomenon is observed. With increasing the drug concentration the CSI path is also affected as the OSI path. As with the increase in the drug concentrations the channels inactivation through the open-state gradually decreases, the population of the inactivated stated gradually decreases and thus during the refractory period that is in presence of base pulses channels re-factorization to resting state via CsB gradually decreases. This is also a

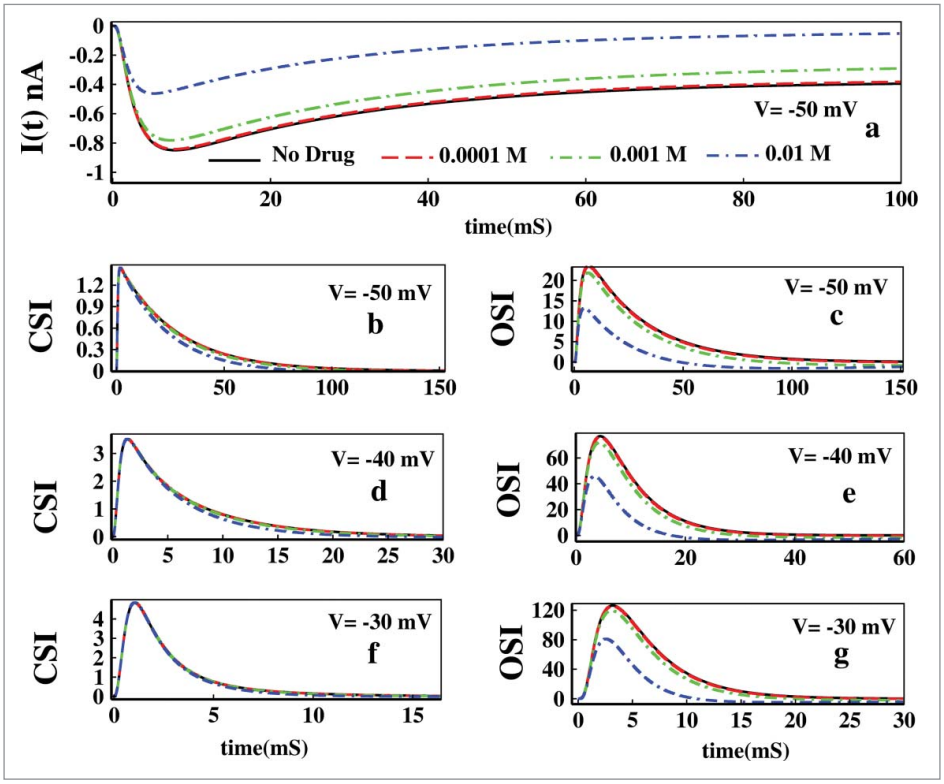

Figure 14. Effect of drug in constant voltage. In (A) ionic current is plotted both without presence of drug and in presence of 0.0001, 0.001, 0.01 M Mexilitine respectively. The left panel of figures (B), (D) and (F) shows the effect of Mexilitine in closed-state inactivation path, whereas the right panel of figures (C), (D) and (G) shows the drug effect on OSI for voltages −50, −40 and −30 mV respectively for aforesaid Mexilitine concentrations.

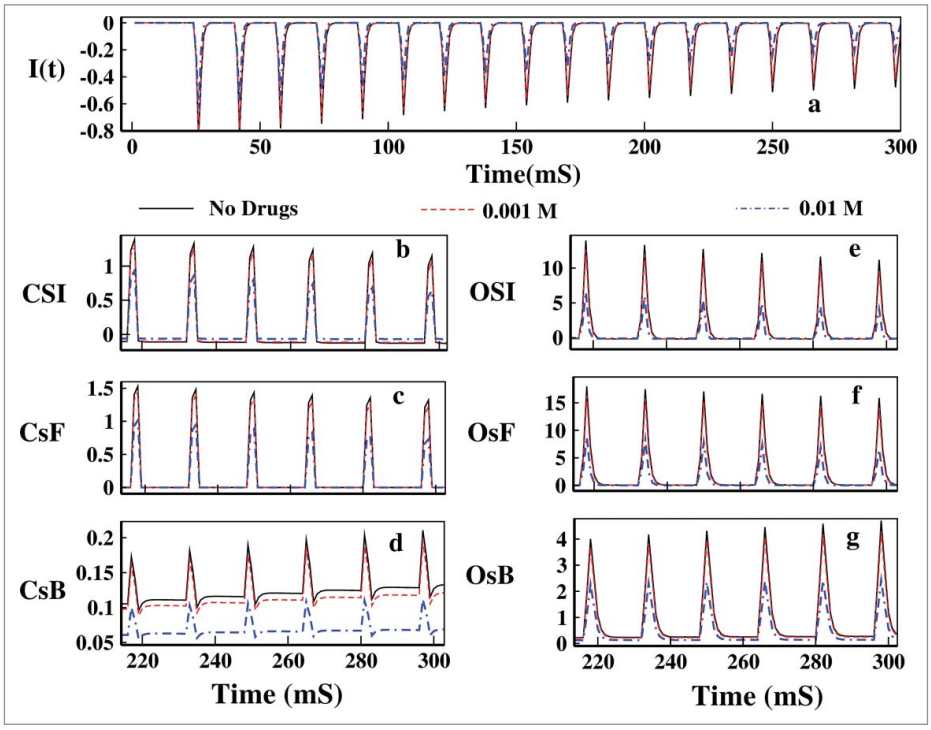

Figure 15. Effect of drug in pulse train. In (A) the ionic current is plotted for 0.001, 0.01 M Mexilitine. In (B), (C) and (D) CSI, CsF and CsB is plotted respectively. In (E), (F) and (G) the OSI, OsF and OsB is plotted for the aforesaid drug concentrations.

cross check of the fact that inactivation occurred via OSI, recovery from inaction occurs via CSI. The gradual decrease in the OSI is due to the gradual increase of the population of the drug bound state P_5^M.

Effect of drug in oscillating voltage protocol

In Figure 16 we have plotted the effect of Mexilitine in presence of oscillating voltage protocol. In Figure 16A

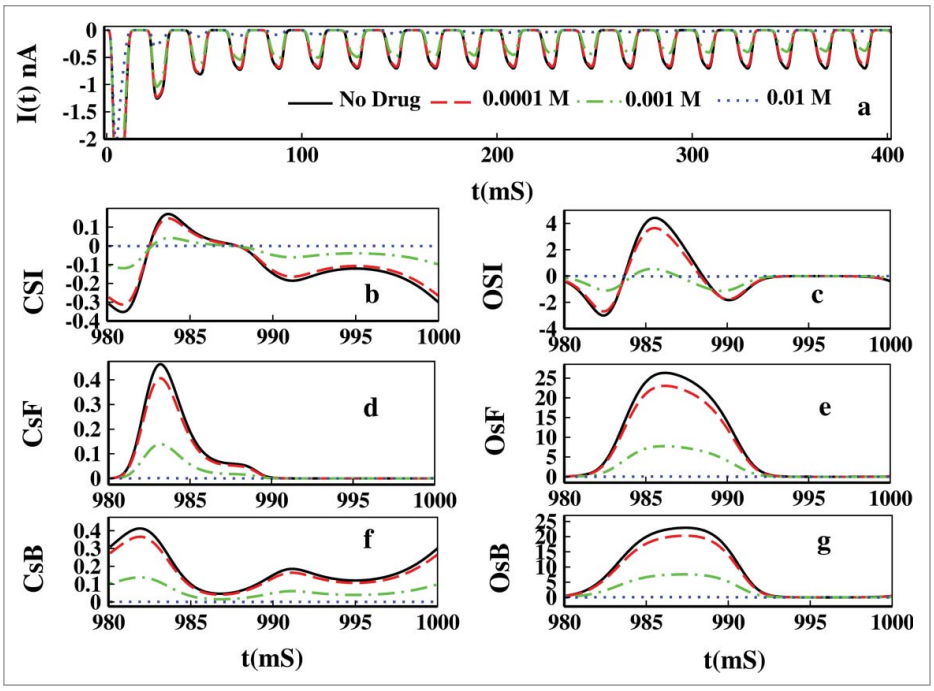

Figure 16. Effect of drug in oscillating voltage. In (A) the ionic current is plotted for 0.0001, 0.001, 0.01 M Mexilitine. In (B), (D) and (E) CSI, CsF and CsB is plotted respectively. In (C), (E) and (G) the OSI, OsF and OsB is plotted for the aforesaid drug concentrations.

we have plotted the ionic current which shows gradual damping of current in presence of Mexilitine. As in the pulse train protocol we see similar explanation for the CSI and OSI to be affected by the increasing drug concentrations. With increasing drug concentration the magnitude of CSI and OSI is decreased.

Conclusion

Inactivation dynamics of sodium channel has been studied here under non-equilibrium environment. By changing the voltage protocols from constant through pulsed to continuously oscillating voltage, we have studied the kinetic flux as well as energetic contributions of the closed and open-state inactivation path. The recently developed non-equilibrium thermodynamic properties used here serves as an improved tool for theoretical understanding of the energetically optimum processes to sustain the auto-regulatory mechanism of inactivation which has not been done earlier. Our approach of non-equilibrium dynamical characterization of inactivation path can invite new avenues in experimental and theoretical research of inactivation, especially for drug blocking and dynamic hysteresis. The conclusions drawn here are mainly as follows.

1. We have characterized the activation and inactivation dominated region of ionic current as a function of voltage.
2. In presence of the constant voltage the path of inactivation is characterized. In a preferential OSI system the OSI path is more favored than CSI for inactivation in moderate to high depolarization. The CSI gradually decrease with increasing depolarizations while OSI increases.
3. From the pulse train analysis it is seen that system follows OSI path to respond to test pulses and comes back to resting states or recovery from inactivation occurs via CSI path during base pulse or refractory period. Recovery from inactivation is relatively a slower process than inactivation and it gradually increases after each pulses with increasing population of inactive states.
4. From the oscillating voltage it is seen that during the hyperpolarised voltage, the system follows CSI path and for depolarized voltage system prefers OSI path.
5. From constant to continuously oscillating voltage protocol, the general conclusion is that during depolarised voltage OSI is most favored path and during hyperpolarised voltage CSI is favored.
6. The results of pulse train and oscillating voltage protocols are both kinetically and thermodynamically established. The calculation of fraction of total epr serves as a supporting tool for theoretical understanding of kinetic results. The thermodynamic results also confirm that these paths show characteristic dynamical hysteretic nature. The study of path of inactivation or the validity of the model gets a strong thermodynamic backup which has not been shown earlier. It is also established that only the kinetic study is not sufficient, the thermodynamic study of inactivation is equally important.
7. For all the voltage protocols, the effect of open-state blocker, Mexilitine shows a characteristic decrease in the relative magnitude of the OSI and CSI path. But the CSI path is least affected by the open-state drug blocking in constant voltage protocol. The dynamical profile of inactivation of the channel can in principle be utilized to estimate the presence of drug and vice versa.

Disclosure of potential conflicts of interest

No potential conflicts of interest were disclosed.

References

[1] Yu FH, Catterall WA. Overview of the voltage-gated sodium channel family. Genome Biol 2003; 4:207; PMID:12620097; http://dx.doi.org/10.1186/gb-2003-4-3-207

[2] Marban E, Yamagishi T, Tomaselli GF. Structure and function of voltage-gated sodium channels. J Physiol 1998; 508:647; PMID:9518722; http://dx.doi.org/10.1111/j.1469-7793.1998.647bp.x

[3] Goldin AL. Mechanisms of sodium channel inactivation. Curr Opin Neurobiol 2003; 13:284-90; PMID:12850212; http://dx.doi.org/10.1016/S0959-4388(03)00065-5

[4] Aldrich RW. Fifty years of inactivation. Nature 2001; 411:643-4; PMID:11395746; http://dx.doi.org/10.1038/35079705

[5] Catterall WA. From ionic currents to molecular mechanisms: the structure and function of voltagegated sodium channels. Neuron 2000; 26:13-25; PMID:10798388; http://dx.doi.org/10.1016/S0896-6273(00)81133-2

[6] Ulbricht W. Sodium Channel Inactivation: Molecular Determinants and Modulation. Physiol Rev 2005;

85:1271-301; PMID:16183913; http://dx.doi.org/10.1152/physrev.00024.2004

[7] Hille B. Ionic channels of excitable membranes. 2nd edition, Sinauer Associates, Sunderland, Mass 1992.

[8] Featherstone DE, Fujimoto E, Ruben PC. A defect in skeletal muscle sodium channel deactivation exacerbates hyperexcitability in human paramyotonia congenita. J Physiol 1998; 506.3:627-38; http://dx.doi.org/10.1111/j.1469-7793.1998.627bv.x

[9] Devor M. Sodium Channels and Mechanisms of Neuropathic Pain. J Pain 2006; 7:S3-S12; PMID:16426998; http://dx.doi.org/10.1016/j.jpain.2005.09.006

[10] Noebels JL. How a Sodium Channel Mutation Causes Epilepsy. Epilepsy Currents 2003; 3:70-1; PMID:15309091; http://dx.doi.org/10.1046/j.1535-7597.2003.03214.x

[11] Kiss T. Persistent Na-channels: origin and function. A review. Acta Biologica Hungarica 2008; 59 (Suppl.):1-12; PMID:18652365; http://dx.doi.org/10.1556/ABiol.59.2008.Suppl.1

[12] Stafstrom CE. Persistent Sodium Current and Its Role in Epilepsy. Epilepsy Curr 2007 Jan; 7(1):15-22; http://dx.doi.org/10.1111/j.1535-7511.2007.00156.x

[13] Aman TK, Grieco-Calub TM, Chen C, Rusconi R, Slat EM, Isom LL, Raman IM. Regulation of Persistent Na Current by Interactions between _ Subunits of Voltage-Gated Na Channels. J Neurosci 2009; 29(7):2027-42; PMID:19228957; http://dx.doi.org/10.1523/JNEUROSCI.4531-08.2009

[14] Catterall WA, Goldin AL, Waxman SG. International Union of Pharmacology. XLVII. Nomenclature and Structure-Function Relationships of Voltage-Gated Sodium Channels. Pharmacol Rev 2005; 57:397-409; PMID:16382098; http://dx.doi.org/10.1124/pr.57.4.4

[15] Hodgkin AL, Huxley AF. The dual effect of membrane potential on sodium conductance in the giant axon of Loligo. J Physiol 1952; 116:497-506; PMID:14946715; http://dx.doi.org/10.1113/jphysiol.1952.sp004719

[16] Aldrich RW, Stevens CF. Inactivation of open and closed sodium channels determined separately. Cold Spring Harbor Symposia on Quantitative Biology 1983; XLVIII:147-53; http://dx.doi.org/10.1101/SQB.1983.048.01.017

[17] Goldman L. Sodium channel inactivation from closed states: evidence for an intrinsic voltage dependency. Biophy J 1995; 69:2369-2377; http://dx.doi.org/10.1016/S0006-3495(95)80106-2

[18] Horn R, Vandenberg CA. Statistical properties of single sodium channels. J Gen Physiol 1984; 84:505-34; PMID:6094703; http://dx.doi.org/10.1085/jgp.84.4.505

[19] Groome JR, Lehmann-Horn F, Holzherr BD. Open and closed-state fast inactivation in sodium channels: Differential effects of a site-3 anemone toxin. Channels 2011; 5 (1):65-78; PMID:21099342; http://dx.doi.org/10.4161/chan.5.1.14031

[20] Armstrong CM, Bezanilla F. Inactivation of the sodium channel. II. Gating experiments. J Gen Physiol 1977; 70:567-90; PMID:591912; http://dx.doi.org/10.1085/jgp.70.5.567

[21] Bahring R, Covarrubias M. Mechanisms of closed-state inactivation in voltage-gated ion channels. J Physiol 2011; 589.3:461-79; http://dx.doi.org/10.1113/jphysiol.2010.191965

[22] Bean BP. Sodium channel inactivation in the crayfish giant axon. Must channels open before inactivating? Biophys J 1981; 35:595-614; PMID:6268217; http://dx.doi.org/10.1016/S0006-3495(81)84815-1

[23] Yellen G. The moving parts of voltage-gated ion channels. Q Rev Biophys 1998; 31:239-95; PMID:10384687; http://dx.doi.org/10.1017/S0033583598003448

[24] Patlak J. Molecular kinetics of voltage-dependent Na + channels. Physiol Rev 1991; 71:1047-80; PMID:1656476

[25] Kuo CC, Bean BP. Na + channels must deactivate to recover from inactivation. Neuron 1994; 12:819-29; PMID:8161454; http://dx.doi.org/10.1016/0896-6273(94)90335-2

[26] Armstrong CM. Na channel inactivation from open and closed states. Proc Nat Aca Sci 2006; 103:17991-6; http://dx.doi.org/10.1073/pnas.0607603103

[27] Millonas MM, Hanck DA. Nonequilibrium response spectroscopy of voltage-sensitive ion channel gating. Biophys J 1998; 74:210-29; PMID:9449324; http://dx.doi.org/10.1016/S0006-3495(98)77781-1

[28] Kargol A, Smithz B, Millonas MM. Applications of Nonequilibrium Response Spectroscopy to the Study of Channel Gating. Experimental Design and Optimization. J Theor Biol 2002; 218:239; PMID:12381295; http://dx.doi.org/10.1006/jtbi.2002.3073

[29] Groot SRD, Mazur P. Non-equilibrium Thermodynamics, North Holland Publ. Comp., Amsterdam 1951.

[30] Kargol A, Hosein-Sooklal A, Constantin L, Przestalski M. Application of oscillating potentials to Shaker potassium channel. Gen Physiol Biophys 2004; 23:53-75; PMID:15270129

[31] Hosein-Sooklal A, Kargol A. Wavelet analysis of non-equilibrium ionic currents in human heart sodium channel (hH1a). J Membr Biol 2002; 188:199-212; PMID:12181611; http://dx.doi.org/10.1007/s00232-001-0188-9

[32] Pal K. Gangopadhyay G, Probing kinetic drug binding mechanism in voltage-gated sodium ion channel: open state versus inactive state blockers. Channels 2015; 9 (5):307-16; PMID:26274618; http://dx.doi.org/10.1080/19336950.2015.1078950

[33] Vandenberg CA, Bezanilla F. A sodium channel gating model based on single channel, macroscopic ionic, and gating currents in the squid giant axon. Biophys J 1991; 60:1511.

[34] Payandeh J, Gamal El-Din TM, Scheuer T, Zheng N, Catterall WA. Crystal structure of a voltage- gated sodium channel in two potentially inactivated states. Nat Lett 2012; 486:136.

[35] Zhang X, Ren W, DeCaen P, Yan C, Tao X, Tang L, Wang J, Hasegawa K, Kumasaka T, He J, et al. Crystal structure of an orthologue of the NaChBac voltage-gated

sodium channel. Nature 2012; vol 486:130; http://dx.doi.org/10.1038/486323e

[36] Schnakenberg J. Network theory of microscopic and macroscopic behavior of master equation systems. Rev Mod Phys 1976; 48:571; http://dx.doi.org/10.1103/RevModPhys.48.571

[37] Jiu-li L, Van den Broeck C, Nicolis G. Stability criteria and uctuations around nonequilibrium states. Z Phys B 1984; 56:165; http://dx.doi.org/10.1007/BF01469698

[38] Nicolis G. Fluctuations around nonequilibrium states in open nonlinear systems. J Stat Phys 1972; 6:195; http://dx.doi.org/10.1007/BF01023688

[39] Seifert U. Entropy Production along a Stochastic Trajectory and an Integral Fluctuation Theorem. Phys Rev Lett 2005; 95:040602; PMID:16090792; http://dx.doi.org/10.1103/PhysRevLett.95.040602

[40] Ge H, Qian H. Physical origins of entropy production, free energy dissipation, and their mathematical representations. Phys Rev E 2010; 81:051133; http://dx.doi.org/10.1103/PhysRevE.81.051133

[41] Das B, Banerjee K, Gangopadhyay G. Entropy hysteresis and nonequilibrium thermodynamic efficiency of ion conduction in a voltage-gatedpotassium ion channel. Phys Rev E 2012; 86:061915; http://dx.doi.org/10.1103/PhysRevE.86.061915

[42] Induction of pseudo-periodic oscillation in voltage gated sodium channel properties is dependent on the duration of the prolonged depolarization. Euro J Neurosci 2004; 20:127-43; http://dx.doi.org/10.1111/j.1460-9568.2004.03466.x

[43] Raman IM, Bean BP. Inactivation and Recovery of Sodium Currents in Cerebellar Purkinje Neurons: Evidence for Two Mechanisms. Biophys J 2001; 80:729-37; PMID:11159440; http://dx.doi.org/10.1016/S0006-3495(01)76052-3

[44] Colbert CM, Magee JC, Hoffman DA, Johnston D. Slow recovery from inactivation of Na+ channels underlies the activity dependent attenuation of dendritic action potentials in Hippocampal CA1 pyramidal neurons. J Neurosci 1997; 17:6512-21; PMID:9254663

[45] Chanda B, Blunck R, Faria LC, Schweizer Mody, Bezanilla F. A hybrid approach to measuring electrical activity in genetically specified neurons. Nature Neuroscience 2005; 8:1619-26; PMID:16205716; http://dx.doi.org/10.1038/nn1558

[46] Olguin IIA, Carrillo E, Islas LD, Lagunas FG. Recovery from slow inactivation of Shab K+ channels. Channels 2013; 7:225-8; PMID:23584197; http://dx.doi.org/10.4161/chan.24585

[47] Kuo CC, Yang S. Recovery from inactivation of T-type Ca2+ channels in rat thalamic neurons. J Neurosci 2001; 21:1884-92; PMID:11245673

[48] Fohlmeister JF, Adelman WJ Jr. Gating current harmonics. I. Sodium channel activation gating in Dynamic Steady states. Biophysci J 1985; 48:375-90; http://dx.doi.org/10.1016/S0006-3495(85)83794-2

[49] Pustovoit MA, Berezhkovskii AM, Bezrukov SM. Analytical theory of hysteresis in ion channels: two-state model. J Chem Phys 2006; 125:194907; PMID:17129167; http://dx.doi.org/10.1063/1.2364898

[50] Sah M Pd, Kim H, Chua LO. Brains Are Made of Memristors. IEEE circuits and systems magazine 2014; 1531-636X.

[51] Scholz A. Mechanisms of (local) anaesthetics on voltage-gated sodium and other ion channels. Br J Anaesth 2002; 89:52-61; PMID:12173241; http://dx.doi.org/10.1093/bja/aef163

[52] Fozzard HA, Lipkind GM. The tetrodotoxin binding site is within the outer vestibule of the sodium channel. Marine Drugs 2010; 8:219-34; PMID:20390102; http://dx.doi.org/10.3390/md8020219

[53] Starmer CF, Lastra AA, Nesterenko VV, Grant AO. Proarrhythmic response to sodium channel blockade. Theoretical model and numerical experiments. Circulation 1991; 84:1364-77; PMID:1653123; http://dx.doi.org/10.1161/01.CIR.84.3.1364

[54] Stramer CF. How antiarrhytmic drugs increase the rate of sudden cardiac death. Int J Bifurcation Chaos 2002; 12:1953; http://dx.doi.org/10.1142/S0218127402005625

[55] Clancy CE, Zhu ZI, Rudy Y. Pharmacogenetics and anti arrhythmic drug therapy: a theoretical investigation. Am J Physiol Heart Circ Physiol 2007; 292:H66-75; PMID:16997895; http://dx.doi.org/10.1152/ajpheart.00312.2006

[56] Fozzard HA, Lipkind GM. The Tetrodotoxin Binding Site Is within the Outer Vestibule of the Sodium Channel. Marine Drugs 2010; 8:219; PMID:20390102; http://dx.doi.org/10.3390/md8020219

[57] Nygren A, Fiset C, Firek L, Clark JW, Lindblad DS, Clark RB, Giles WR. Mathematical mode of an adult human atrial cell: The role of K^+ currents in repolarization. Cir Res 1998; 82:63-81; http://dx.doi.org/10.1161/01.RES.82.1.63

[58] MacCannell KA, Bazzazi H, Chilton L, Shibukawa Y, Clark , Giles WR. A mathematical model of electronic interactions between ventricular myocytes and fibroblasts. Biophys J 2007; 92:4121-32; PMID:17307821; http://dx.doi.org/10.1529/biophysj.106.101410

[59] Clancy CE, Tateyama M, Liu H, Wehrens XHT, Kass RS. Noneqilubrium gating in cardiac Na+ channels: an original mechanism of arrhythmia. Circulation 2003; 107:2233-7; PMID:12695286; http://dx.doi.org/10.1161/01.CIR.0000069273.51375.BD

[60] Clancy CE, Kass RS. Theoretical investigation of the neuronal Na+ channel SCN1A: Abnormal gating and epilepsy. Biophys J 2004; 86:2606-14; PMID:15041696; http://dx.doi.org/10.1016/S0006-3495(04)74315-5